Taylor & Francis
Taylor & Francis Group

RESEARCH ARTICLE

🔓 OPEN ACCESS   Check for updates

Functional recovery in photo-damaged human dermal fibroblasts by human adipose-derived stem cell extracellular vesicles

Ji Suk Choi[a,b]*, Woo Lee Cho[a]*, Yeo Jin Choi[a], Jae Dong Kim[b], Hyun-A Park[b], Su Yeon Kim[b], Jae Hyung Park[c], Dong-Gyu Jo[d] and Yong Woo Cho[a,b]

[a]Department of Chemical Engineering, Hanyang University, Ansan, Republic of Korea; [b]Research Institute, Exostemtech Inc, Ansan, Republic of Korea; [c]School of Chemical Engineering, Sungkyunkwan University, Suwon, Republic of Korea; [d]School of Pharmacy, Sungkyunkwan University, Suwon, Republic of Korea

ABSTRACT

Ultraviolet-B (UVB) irradiation causes imbalance between dermal matrix synthesis and degradation through aberrant upregulation of matrix metalloproteinases (MMPs), which leads to overall skin photoaging. We investigated the effects of extracellular vesicles (EVs) derived from human adipose-derived stem cells (HASCs) on photo-damaged human dermal fibroblasts (HDFs). EVs were isolated from conditioned media of HASCs with tangential flow filtration and characterized using transmission electron microscopy (TEM), nanoparticle tracking analysis (NTA), western blotting, micro RNA (miRNA) arrays, cytokine arrays and liquid chromatography coupled with tandem mass spectrometry (LC-MS/MS). The effects of EVs on the UVB-irradiated HDFs were evaluated using scratch assay, ELISA and real-time PCR. Microarrays exhibited that EVs are rich in various miRNAs and proteins, and that these EV contents are linked to a broad range of biological functions, including fibroblast proliferation, UV protection, collagen biosynthesis, DNA repair and cell ageing. A scratch assay showed that HASC-EVs enhanced the migration ability of UVB-irradiated HDFs. Real-time RT-PCR and ELISA analyses revealed that the HASC-derived EVs significantly suppressed the overexpression of MMP-1, -2, -3 and -9 induced by UVB irradiation and enhanced the expression of collagen types I, II, III and V and elastin. In particular, tissue inhibitor of metalloproteinase (TIMP)-1 and transforming growth factor (TGF)-β1, which are important factors involved in MMP suppression and ECM synthesis, were upregulated in EV-treated HDFs after UVB irradiation. Overall results suggest that diverse components that are enriched in HASC-derived EVs could act as a biochemical cue for recovery from skin photoaging.

Introduction

Skin ageing is a complex biological phenomenon that is caused by intrinsic and extrinsic factors. The intrinsic ageing reflects naturally occurring changes in the skin with age and extrinsic ageing is affected by environmental factors such as sunlight, air pollution, chemicals and toxins [1]. Ultraviolet (UV) radiation is one of the most harmful environmental factors that accelerate ageing. Repeated exposure to UV radiation, in particular UVB radiation, produces reactive oxygen species (ROS) that promote collagen and elastin breakdown by upregulating matrix metalloproteinases (MMPs), thereby leading to photoaging, which is characterized by wrinkles, dryness, loss of elasticity and pigmentation [2,3]. Various single or complex ingredients, such as anti-oxidants, retinoids, peptides, growth factors, extracts and cell conditioned medium, have been developed from natural or synthetic sources to protect or repair the skin [4–9]. Driven by the demands of a population of increasing age [10,11], recent studies have focused on the development of new ingredients with advanced functions combining cosmetic and pharmaceutical properties.

Recently, extracellular vesicles (EVs) have been the spotlight as a therapeutic candidate for skin regeneration. EVs are small membrane vesicles (30–200 nm in diameter) secreted by various cell types through the fusion of multi-vesicular bodies (MVBs) with the plasma membrane [12,13]. EVs can shuttle genetic materials, transcription factors and functional peptides or proteins, implicating their role in cell-to-cell communication and modulating the molecular activities of recipient cells [14–17]. Several groups have shown that stem cell or progenitor cell-derived exosomes are effective for cutaneous wound healing [18–22]. In addition

---

to these exosome types, other studies have shown that keratinocyte-derived exosomes contribute to wound healing by regulating gene expression in dermal fibroblasts [23]. In this study, we investigated the effects of EVs secreted from human adipose-derived stem cells (HASCs) on in vitro UVB-induced photoaging models. The HASC-derived EVs were characterized in terms of concentration and morphology using transmission electron microscopy (TEM) and nanoparticle tracking analysis (NTA). The EV markers were characterized using western blotting, and the internal contents were analysed using micro RNA (miRNA) arrays, cytokine arrays and liquid chromatography coupled with tandem mass spectrometry (LC-MS/MS). We evaluated the effects of HASC-derived EVs on the expression of genes and proteins associated with dermal matrix synthesis and degradation in UVB-irradiated human dermal fibroblasts (HDFs).

Materials and methods

Extracellular vesicles (EVs) isolation from human adipose-derived stem cells (HASCs)

Primary HASCs were purchased from Cefobio Inc. (Seoul, Korea). The HASCs were maintained in growth medium (Dulbecco's Modified Eagle's Medium (DMEM) supplemented with 10% foetal bovine serum (FBS) and 1% penicillin streptomycin (P/S)) at 37°C in humidified air containing 5% CO_2. Cell culture media, FBS and antibiotics were purchased from Life Technologies (Carlsbad, CA, USA). Conditioned medium (CM) was collected from proliferating HASCs (passages 7–9) and used for EV isolation (Figure 1(a)). Briefly, HASCs were seeded at a concentration of 1×10^6 cells per flask into five T-175 flasks. After 4 days of culture (2×10^6 cells per flask), the cells were washed with phosphate-buffered saline (PBS), and the medium was replaced with serum-free DMEM for 24 h. The CM (500 mL) was collected, and the cell debris was removed via centrifugation at $300 \times g$ for 10 min, followed by passage through a 0.22-μm filter (Millipore, Billerica, MA, USA). The CM was concentrated using tangential flow filtration (TFF) with a 500-kDa MWCO ultrafiltration membrane filter capsule (Pall Corporation, Port Washington, NY, USA). The CM was continuously pumped through the membrane filter system and circulated at a rate of 4 mL/min. The sample was serially concentrated via TFF to remove contaminants smaller than the 500-kDa MWCO. The EVs were kept in circulation as the retentate and concentrated in a 50 mL disposable tube to a final volume of approximately 10 mL. Particle concentration and size distribution were measured using a NanoSight LM10 (Malvern Instruments Ltd., UK). The samples were diluted 10- to 20-fold with PBS to reach the optimal concentration for instrument linearity (20–30 particles/frame), and readings were performed in triplicates of 30 s at 30 frames per second. The EV proteins was quantified using the Pierce BCA Protein Assay Kit (Thermo Scientific, Rockford, IL, USA) according to the manufacturer's instruction, and the EVs were stored at − 70°C until further use.

Transmission electron microscopy (TEM)

The EVs were fixed in 0.5% glutaraldehyde solution and incubated overnight at 4°C. The samples were dehydrated with absolute ethanol for 10 min, and were collected on formvar/carbon-coated copper grids (Samchang Inc., Korea). The grids were contrasted with 1% phosphotungstic acid for 1 min and washed with absolute ethanol. The grids were dried completely and imaged using TEM (JEM-2100F, JEOL Ltd., Japan). For cryo-TEM, an aliquot of concentrated EVs was applied to lacey carbon grid (Electron Microscopy Science, Hatfield, PA, USA). The grids were stored in liquid nitrogen, then transferred to cryospecimen holder and maintained at −180°C. Images were collected at a magnification of 18,000 x to 29,000 x on the Tecnai F20 Twin transmission electron microscope operating at 200 kV.

Western blot analysis

HASC-derived EVs were lysed in RIPA buffer (25 mM Tris-HCl, pH 7.6, 150 mM NaCl, 0.5% Triton X-100, 1% Na-deoxycholate, 0.1% sodium dodecyl sulphate and protease inhibitor cocktail). A total of 20 μg of protein was electrophoresed in a 10% SDS-PAGE gel and transferred to a PVDF membrane (Bio-Rad, Hercules, CA, USA). The membrane was blocked with 5% BSA in T-TBS (10 mM Tris, 150 mM NaCl and 0.1% Tween 20) for 2 h at room temperature and incubated with primary antibodies against TSG101, CD9, CD63, CD81, GM130, Calnexin and β-actin (Abcam, Cambridge, UK) overnight at 4°C. After vigorous washing in TBS-T, the membrane was incubated with horseradish peroxidase (HRP)-tagged secondary antibodies (Santa Cruz Biotechnology, Dallas, TX, USA) for 2 h. The labelled proteins were visualized on X-ray film (AgfaPhoto, Germany) using a developer and fixer (VIVID, Korea). All chemical reagents and protease inhibitor cocktails were purchased from Sigma-Aldrich (St. Louis, MO, USA).
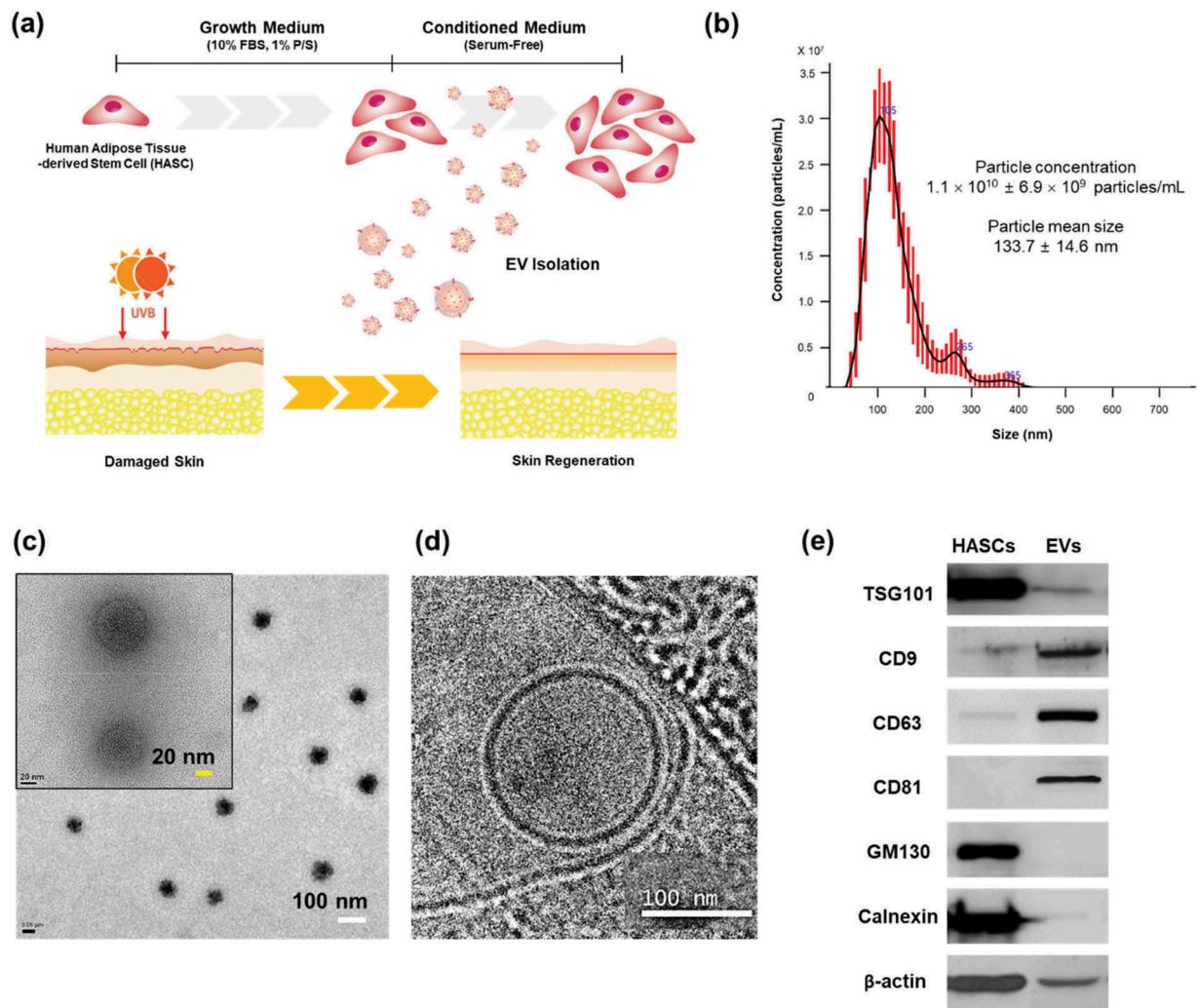
Figure 1. Characterization of EVs secreted from HASCs. (a) Schematic representations of EV isolation from HASCs and the EV treatment of UVB-induced skin ageing. (b) Nanoparticle tracking analysis (NTA) showing the concentration of the EVs. (c) Classic and (d) cryogenic transmission electron microscope (TEM) pictures of EVs. The scale bars represent 100 nm (white) and 20 nm (yellow). (e) Western blot analysis of EVs. Expression of EV markers (TSG101, CD9, CD63 and CD81) and internal protein markers (GM130 and Calnexin).

MicroRNA (miRNA) analysis

Total RNA was extracted from EVs using the RNeasy Mini kit (Qiagen, Germany). The purity of the RNA was assessed using a Nanodrop spectrophotometer (ThermoFisher Scientific), and the miRNA analysis was performed by Biocore Co. (Seoul, Korea). EV RNA integrity was determined using an Agilent 2100 Bioanalyzer (Santa Clara, CA, USA). Human miRNA was analysed using an Affymetrix GeneChip miRNA 4.0 array (ThermoFisher Scientific). Specifically, total RNA (1 µg per sample) was labelled using the FlashTag™ Biotin RNA Labeling Kit (Thermo Fisher Scientific), and the samples were hybridized on the arrays for 18 h at 48°C. The arrays were washed to remove non-specifically bound nucleic acids, stained using a Fluidics Station 450, and scanned using the GeneChip Scanner 3000 7G system (Affymetrix). Finally, differentially expressed miRNA was automatically analysed using the Affymetrix Expression Console software, version 1.4.1. Functional analysis of the miRNA was performed using publicly available algorithms including Cluster, version 3.0; TreeView; GeneSpring, version 13.1.1; and TargetScan, version 6.2. The gene ontology biological process (GO-BP) terms and KEGG pathway terms that were enriched in the predicted target genes were determined using DAVID Bioinformatics Resources, version 6.7.

Cytokine array

The cytokines in the EVs were analysed using a human 80-cytokine array kit (AAH-CYT-G5) for HASC-derived

EVs according to the manufacturer's protocol (RayBiotech, Norcross, GA, USA). A glass chip containing various human cytokine antibodies was blocked with blocking buffer and incubated with EV lysates (total protein 10 μg). The glass chip was washed and subsequently treated with biotin-conjugated antibodies. After incubation with fluorescent dye-conjugated streptavidin, the cytokine signals were detected using a laser scanner (Molecular Devices, CA, USA) operating on the Cy3 channel (excitation frequency = 532 nm). Signal intensities were quantified with GenePix Pro software (Molecular Devices, CA, USA).

Ultraviolet B (UVB) irradiation of human dermal fibroblasts (HDFs)

HDFs were obtained from ATCC (CRL-2522, Manassas, VA, USA). The HDFs were seeded in 24-well plates at 1×10^5 cells per well and maintained in growth medium (GM, DMEM containing 10% FBS and 1% P/S) incubated at 37°C for 24 h under 5% CO_2 until they reached 90% confluence. For UVB irradiation, the HDFs were washed with PBS and exposed to UVB for 10 s at a dose of 0.05 J/cm^2 with a spectral peak of 302 nm (EL Series UV lamp 8W, UVP, Upland, CA, USA) once a day for 3 days. All cells were washed with PBS and incubated for 24 h in serum-free DMEM with or without EVs at 1×10^8 particles/mL. Control cells were kept in growth medium (10% FBS) without UVB exposure. The cells and supernatants were collected for quantitative RT-PCR and ELISAs, respectively.

EV labelling and cellular uptake

HASC-derived EVs were labelled with PKH67 (Sigma, St. Louis, MO, USA) for 30 s at room temperature. Unreacted PKH67 dyes were removed with column (MWCO 3000 Da, Invitrogen, CA, USA). Normal HDFs and UVB-irradiated HDFs were incubated at 37°C with labelled EVs (1×10^8 particles/mL) for 3 h, and then observed with a confocal microscope (Leica TCS SP8, Leica Microsystems, Buffalo Grove, IL, USA).

Scratch closure test

The HDFs were seeded at 1×10^5 cells per well in 24-well plates and cultured at 37°C under 5% CO_2. The cells were irradiated with UVB light for 3 days and then scratched at a consistent length using a sterilized 200-μL disposable pipette tip. The cells were washed with PBS and maintained in GM, serum-free medium (SFM), BSA 0.1% or EVs (1×10^8 particles/mL) containing SFM. Images of the scratched areas were produced at 0 and 24 h and the area between the two edges of the wound was measured using Adobe Photoshop 6.0 (Adobe System Software Ireland Ltd., Ireland) from three independent experiments. The edges of the wound at same regions were distinguished using the magnetic lasso tool of Photoshop to calculate the wound area.

Transwell migration assay

The HDFs were irradiated with UVB light for 3 days. For transwell migration assay, the normal and UVB-irradiated HDFs were plated at 5×10^4 cells/100 μL in GM onto upper chambers in transwell insert (Corning, NY, USA) and 600 μL of different media (GM, SFM, BSA 0.1% or EVs containing SFM) were added to the lower chamber. After incubation for 24 h at 37°C, non-migrating cells were removed with cotton swabs. Cells at the bottom of the membrane were fixed with 4% paraformaldehyde and stained with crystal violet solution for 15 min. Stained cells were visualized under a microscope.

Proliferation assay

Cell proliferation was evaluated using Cell Counting Kit-8 (Dojindo Molecular Technologies, Inc., Rockville, MD, USA). The HDFs were irradiated with UVB light for 3 days. The normal and UVB-irradiated HDFs were seeded at 3×10^4 cells in 24-well plates and cultured for 48 h at 37°C under 5% CO_2. 10 μL of CCK-8 reagent was added to each well and incubated for 1 h. Absorbance readings were then taken at 450 nm using a microplate spectrophotometer (BioTek Instruments, Winooski, VT, USA).

Quantitative RT-PCR

Primers for *MMP-1, MMP-2, MMP-3, MMP-9, COL1A1, COL2A1, COL3A1, COL4A2, COL5A1, ELN, TIMP-1* and *TGFβ1* were purchased from SABiosciences (Valencia, CA). Total RNA was extracted from the cells using the RNA-spin™ Total RNA Extraction Kit (iNtRon Biotechnology Inc., Korea) according to the manufacturer's instructions. cDNA was synthesized from 500 ng of total RNA using the RT^2 First Strand Kit (Qiagen, Hilden, Germany). The genes were simultaneously amplified using a Stratagene Mx3000P (Agilent Technologies, Santa Clara, CA, USA) with the thresholds and baselines set according to the manufacturer's instructions. The fold change in gene expression (compared to the controls) was calculated using SABiosciences webportal software.

ELISA

MMP-1 -3, -9, type 1 procollagen, type 3 collagen and TIMP-1 were quantified via enzyme-linked immunosorbent assays (ELISAs) according to the manufacturer's protocol (Abcam). The absorbance was measured at 450 nm using a microplate spectrophotometer.

Statistical analysis

The experimental data are presented as mean ± standard deviation (SD). Student's two-tailed t-test and 2-way ANOVA were performed using GraphPad Prism 7 software (San Diego, CA, USA). The P values are shown in the figures.

Results

Characterization of HASC-derived EVs

Various methods (eg ultracentrifugation, density gradients, precipitation, size-exclusion chromatography and tangential flow filtration) have been proposed for isolation and purification of EVs. Each of these methods has advantages and limitations, regarding EV purity, reproducibility, efficiency, and scalability [24]. In this study, EVs were isolated using TFF with 500-kDa MWCO ultrafiltration membrane filter. The TFF is a rapid, efficient and automated system for large-scale production of EVs. However, the purity of EVs isolated by TFF may vary depending on process conditions, such as filter molecular weight cut-off and diafiltration cycles [25,26]. Based on our results, the TFF system is applicable to EV isolation and purification. EVs isolated from HASCs were characterized in terms of particle concentration, morphology and surface markers (Figure 1). The mean particle diameter was 133.7 ± 14.6 nm and particle concentration was $1.1 \times 10^{10} \pm 6.9 \times 10^{9}$ particles/mL (Figure 1(b)). Particles were also characterized under classic (Figure 1(c)) and cryo-TEM (Figure 1(d)). EVs displayed a round shape with bilayer structure. Western blotting revealed that the EVs were positive for EV markers including TSG101, CD9, CD63 and CD81, while non-EV markers, GM130 and Calnexin were not detected (Figure 1(e)).

Expression profiling of EV miRNAs

To profile the EV miRNAs, total RNA was isolated from HASC-derived EVs and analysed using GeneChip miRNA 4.0 arrays from Affymetrix including probes for 2578 mature human miRNAs (Figure 2). In total, 577 miRNAs were expressed above the normalized signal intensity (log2 value) to the negative control probe signal. To better understand the function of the miRNAs

differentially expressed in HASC-derived EVs, gene ontology (GO) annotation was performed using DAVID, version 6.8 (http://david.abcc.ncifcrf.gov) with a standard Benjamini value < 0.05. We selected the top 10 GO terms of molecular functions (MF), cellular components (CC), and biological processes (BP). The predicted functions included various binding, transcription factor activities, and enzymatic activity. The predicted cellular components of miRNAs included the nucleoplasm (30.1), nucleus (23.4), cytosol (17.3), membrane (14.2) and extracellular exosome (4.1). The predicted biological process included transcription regulation (13.3), cellular response to DNA damage stimulus (4.3), the Wnt signalling pathway (3.6), regulation of cell cycle (3.2), extracellular organization (3.1), cell migration (3.1) and cell ageing (2.1). A Kyoto Encyclopedia of Genes and Genomes (KEGG) pathway annotation was performed based on scoring and visualization of the pathways collected in the KEGG database (http://www.genome.jp/kegg). The top 12 pathways were involved in the Hippo signalling pathway (8.7), pathways in caner (7.8), signalling pathways regulating stem cells (6.5), the Wnt signalling pathway (5.0), TGF-beta signalling pathway (4.5), cell cycle (4.4), the adherens junction (4.2) and mitogen-activated protein kinase (MAPK) signalling pathway (3.4). The roles of the EV miRNAs, along with their corresponding validated target genes, are schematically represented in Figure 2(b). From these results, we suggest that HASC-derived EVs contain miRNAs that can activate or suppress multiple genes involved in fibroblast proliferation, UV protection, collagen biosynthesis, DNA repair and cell ageing, thereby contributing to the functional recovery of UVB-irradiated HDFs.

Proteomic analysis and antibody-based arrays of EV proteins

The EV proteins were analysed using LC-MS/MS. We identified 116 proteins including 76 EV proteins identified in the ExoCarta database (Supplementary Table S1). The EV proteins were categorized by molecular function and biological process using GO analysis in DAVID Bioinformatics Resources, version 6.8 (Figure 3(a) and Supplementary Table S2). The main molecular functions of the identified proteins were protein binding (44.8%), enzyme activity (6.0%), ion binding (6.0%), ECM structural constituent (4.3%) and DNA binding (1.7%). The biological processes are related to ECM organization (8.6%), signalling pathway (7.8%), cell migration (6.9%), cell proliferation (6.9%), transport (6.9%), inflammatory response (6.0%), cell differentiation (3.4%), regulation of gene expression (3.4%),
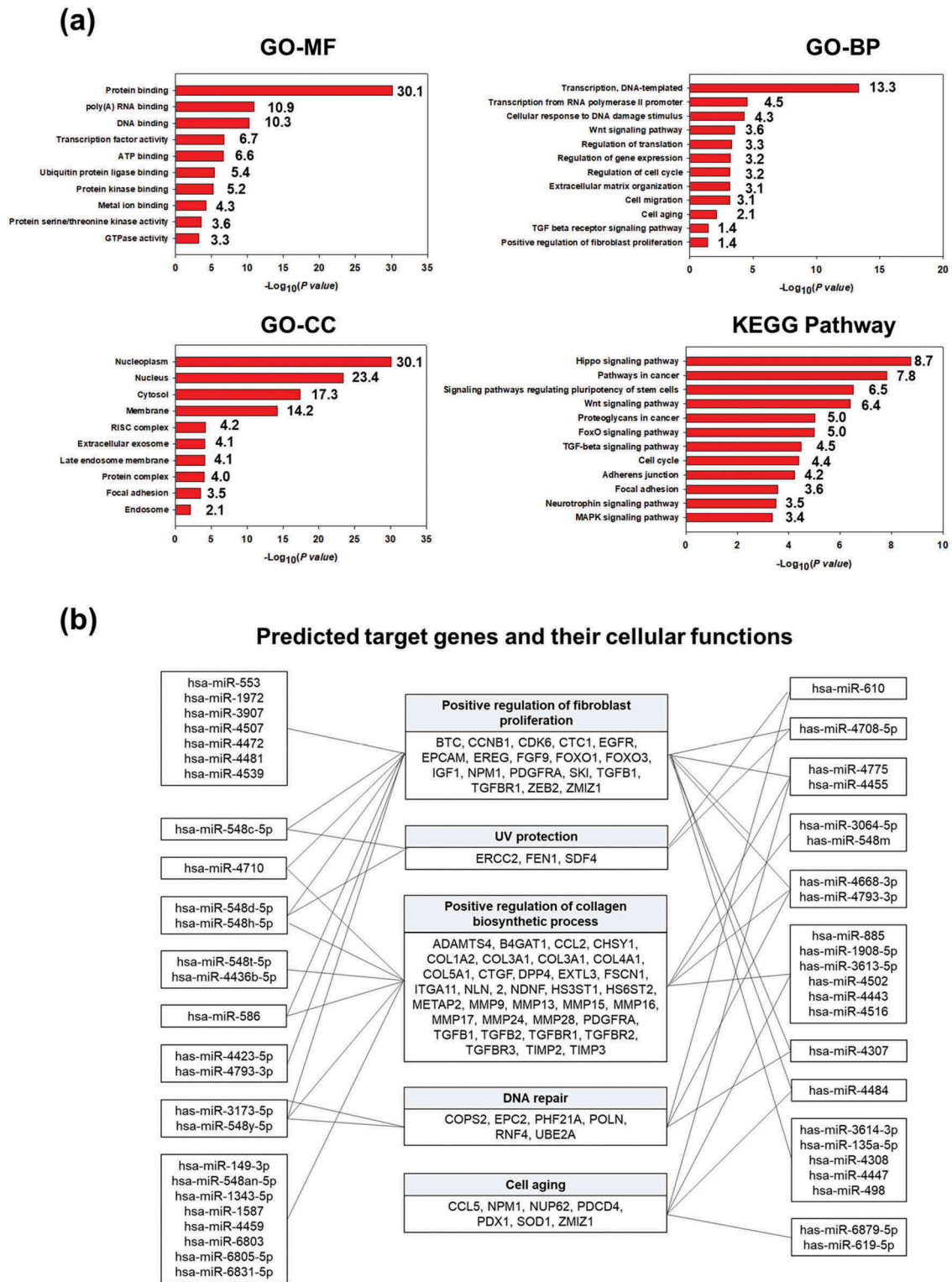
Figure 2. miRNA profiling of HASC-derived EVs. (a) Gene target analysis of miRNA profile of HASC-derived EVs. (b) Schematic representation of the predicted target genes and corresponding cellular functions of the miRNAs enriched in EVs.

angiogenesis (2.6%), cytokine production (2.6%), keratinization (2.6%) and apoptosis (0.9%), suggesting that HASC-derived EVs play a functional role in protein production and cellular behaviours.

The cytokines in the EVs were detected using human cytokine antibody arrays. In total, 61 of the 80 cytokines were found at marked levels (Figure 3(b)). Of those, 15 cytokines involved in
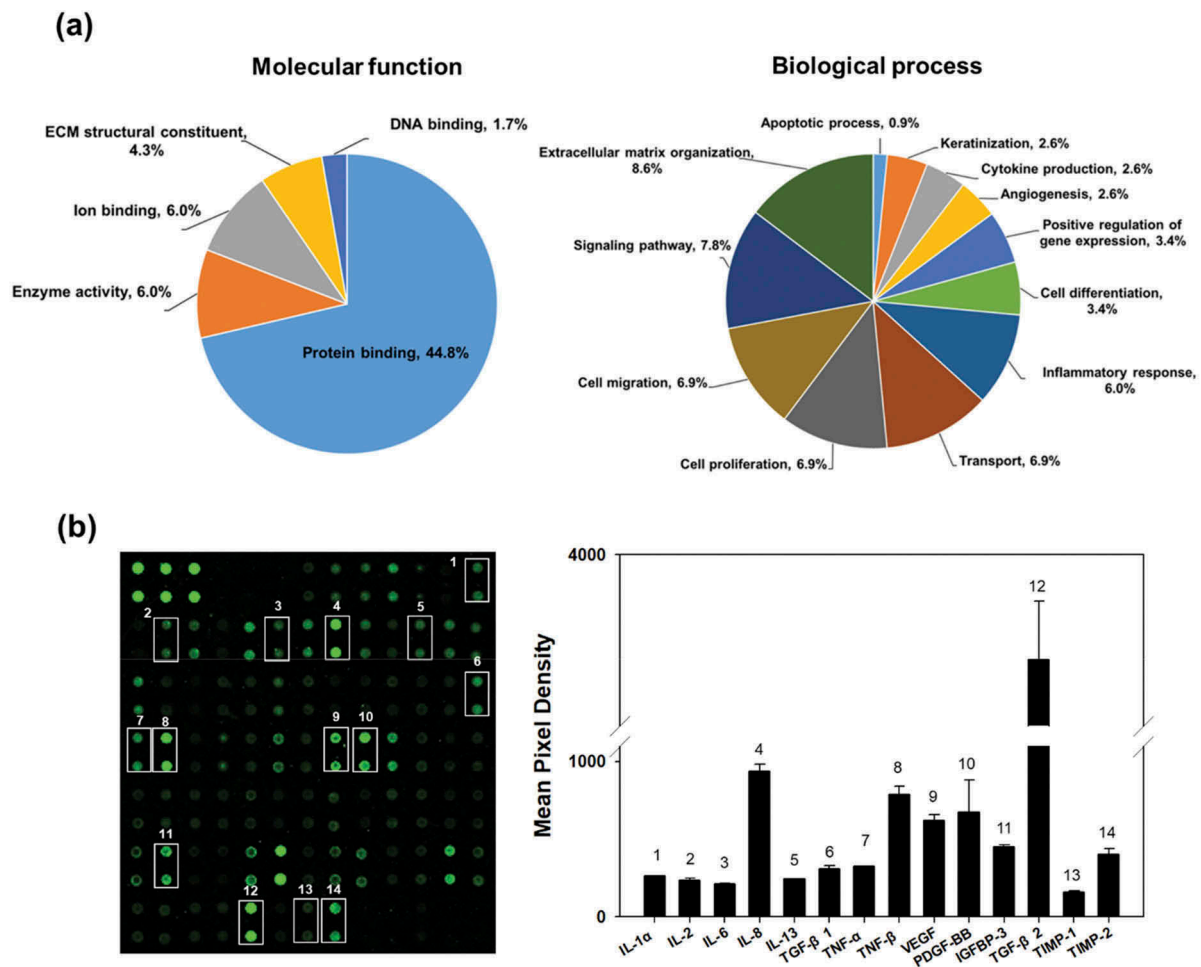
Figure 3. Proteomic analysis and cytokine arrays of HASC-derived EVs. (a) Pie chart depicting the functional classification of the proteins differentially expressed in EVs. EV proteins were categorized by molecular function and biological process using GO analysis in DAVID Bioinformatics Resources, version 6.8. (b) Representative fluorescent images of the cytokine arrays. Cytokines were arrayed on a glass chip containing 80 different cytokine antibodies and detected with a laser scanner using the Cy3 channel. Quantitation of the signals was performed via image analysis. The signal intensity was normalized to the positive control and expressed as fold change. The mean relative intensities and standard deviations are based on two different experiments. Abbreviations: IGF-1, insulin-like growth factor-1; IGFBP, insulin-like growth factor-binding protein; IL, interleukin; MCP-1, monocyte chemotactic protein 1; PDGF-BB, platelet-derived growth factor-BB; TGF-β1, transforming growth factor-beta1; TIMP, tissue inhibitor of metalloproteinase; TNF, tumour necrosis factor; VEGF, vascular endothelial growth factor.

proliferation and collagen synthesis in fibroblasts were expressed in EVs including interleukin-1 alpha, -2, -6, -8 and -13 (IL-1a, IL-2, IL-6, IL-8 and IL-13), transforming growth factor-beta 1 and 2 (TGF-β1 and TGF-β2), tumour necrosis factor-alpha and – beta (TNF-α and TNF-β), vascular endothelial growth factor (VEGF), platelet-derived growth factor-BB (PDGF-BB) and insulin-like growth factor binding protein-3 (IGFBP-3). Additionally, tissue inhibitors of metalloproteinases-1 and -2 (TIMP-1 and TIMP-2), which act as inhibitors of metalloproteinases (MMPs), were expressed in the EVs [27].

Effects of HASC-derived EVs on the migration of UVB-irradiated HDFs

Normal HDFs were incubated with serum-free medium and HASC-derived EVs at various concentrations ranging from 0.1 to 5×10^8 particles/mL for 72 h. HASC-derived EVs significantly affected type I collagen synthesis in normal HDFs in a dose-dependent manner. The collagen synthesis ability of normal HDFs substantially increased in the presence of EVs, with the highest collagen synthesis observed in the presence of 5×10^8 particles/mL of EVs. The collagen synthesis level of UVB-irradiated HDFs was also increased in the presence of

EVs; however, there were no significant differences at a concentration of 1 and 5×10^8 particles/mL EVs (Supplementary Figure S3). Therefore, the EV concentration of 1×10^8 particles/mL was used for the following experiments. To study the cellular uptake of HASC-derived EVs at early time points, normal and UVB-irradiated HDFs were incubated with 1×10^8 particles/mL of fluorescent dye-labelled EVs (green) for 3 h. EVs were internalized into the cytoplasm of both normal and UVB-irradiated HDFs within 3 h (Figure 4). These results imply that HASC-derived EVs are successfully transferred into HDFs with high cellular uptake efficiency.

To investigate the effect of HASC-derived EVs on the migration of HDFs irradiated with UVB, a scratch wound healing and transwell migration assay were performed. The results showed that the UVB-irradiated HDFs exhibited overall slower wound recovery than normal HDFs. However, scratch wounds in UVB-irradiated HDFs treated with EVs closed more rapidly than those in HDFs without EVs or BSA 0.1% treatment (Figure 5). The migration-promoting effect of EVs was also demonstrated in a transwell migration assay (Figure 6(a)). The normal and UVB-irradiated HDFs were loaded on the upper side chamber of a transwell. Each lower chamber was filled with the different media (GM, SFM, BSA 0.1% or EVs containing SFM), respectively. After 24 h, normal HDFs migrated to the lower chamber containing GM or EVs across the membrane. UVB-irradiated HDFs showed a low migration tendency compared to the normal HDFs. Nevertheless, UVB-irradiated HDFs migration into the bottom chamber was more stimulated in the presence of EVs. As shown in Figure 6(b), EVs stimulated the proliferation of UVB-irradiated HDFs. EVs enhanced the proliferation rate of UVB-irradiated HDFs at 48 h,

while no difference was found in the effect of SFM and BSA containing SFM on UVB-irradiated HDFs. These results suggest that HASC-derived EVs improve the migration and proliferation of HDFs that have been reduced by UVB irradiation.

Effects of HASC-derived EVs on the expression of genes and proteins associated with dermal matrix remodelling in UVB-irradiated HDFs

We assessed the synthesis and degradation of dermal matrix-associated proteins and genes in UVB-irradiated HDFs at 24 h after UVB exposure using quantitative RT-PCR (Figure 7) and ELISA (Figure 8). Quantitative real-time RT-PCR showed that UVB irradiation induced a significant increase in *MMP-1* (1.66-fold), *MMP-2* (1.45-fold), *MMP-3* (2.41-fold) and *MMP-9* (2.69-fold) mRNA expression levels compared to the control HDFs, whereas the mRNA levels of other genes were either decreased or similar to that in the control (*COL1A1*; 0.95-fold, *COL2A1*; 0.42-fold, *COL3A1*; 0.79-fold, *COL4A2*; 0.91-fold, *COL5A1*; 0.69-fold, *ELN*; 0.94-fold, *TIMP-1*; 1.26-fold, and *TGFβ1*; 0.84-fold). The HASC-derived exosome treatment significantly inhibited the MMP gene expression induced by UVB irradiation (*MMP-1*; 0.41-fold, *MMP-2*; 1.16-fold, *MMP-3*; 0.71-fold, and *MMP-9*; 1.91-fold). The mRNA expression levels of genes related to dermal matrix synthesis, including *COL1A1* (2.1-fold), *COL2A1* (1.74-fold), *COL3A1* (1.82-fold), *COL5A1* (1.12-fold), *ELN* (1.29-fold), and *TIMP-1* (2.29-fold) were significantly upregulated by the exosome treatment. Interestingly, the mRNA level of *TGFβ1*, a key mediator of type I collagen production [28], was increased after the exosome treatment (1.27-fold).
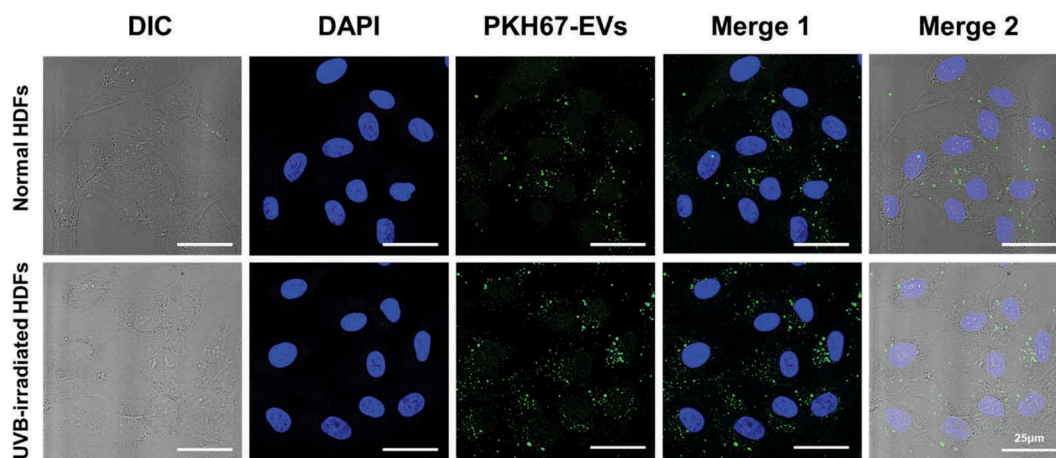

Figure 4. The cellular uptake of HASC-derived EVs in normal and UVB-irradiated HDFs. Light differential interference contrast (DIC) and corresponding confocal images of HDFs after 3 h incubation with 1×10^8 particles/mL of PKH67-labelled EVs, respectively (n = 3). Images of PKH67-labelled EVs (green) with DAPI (blue) were visualized by merging the confocal images (Merge1) or bright-field with confocal images (Merge2). Scale bars represent 25 μm.
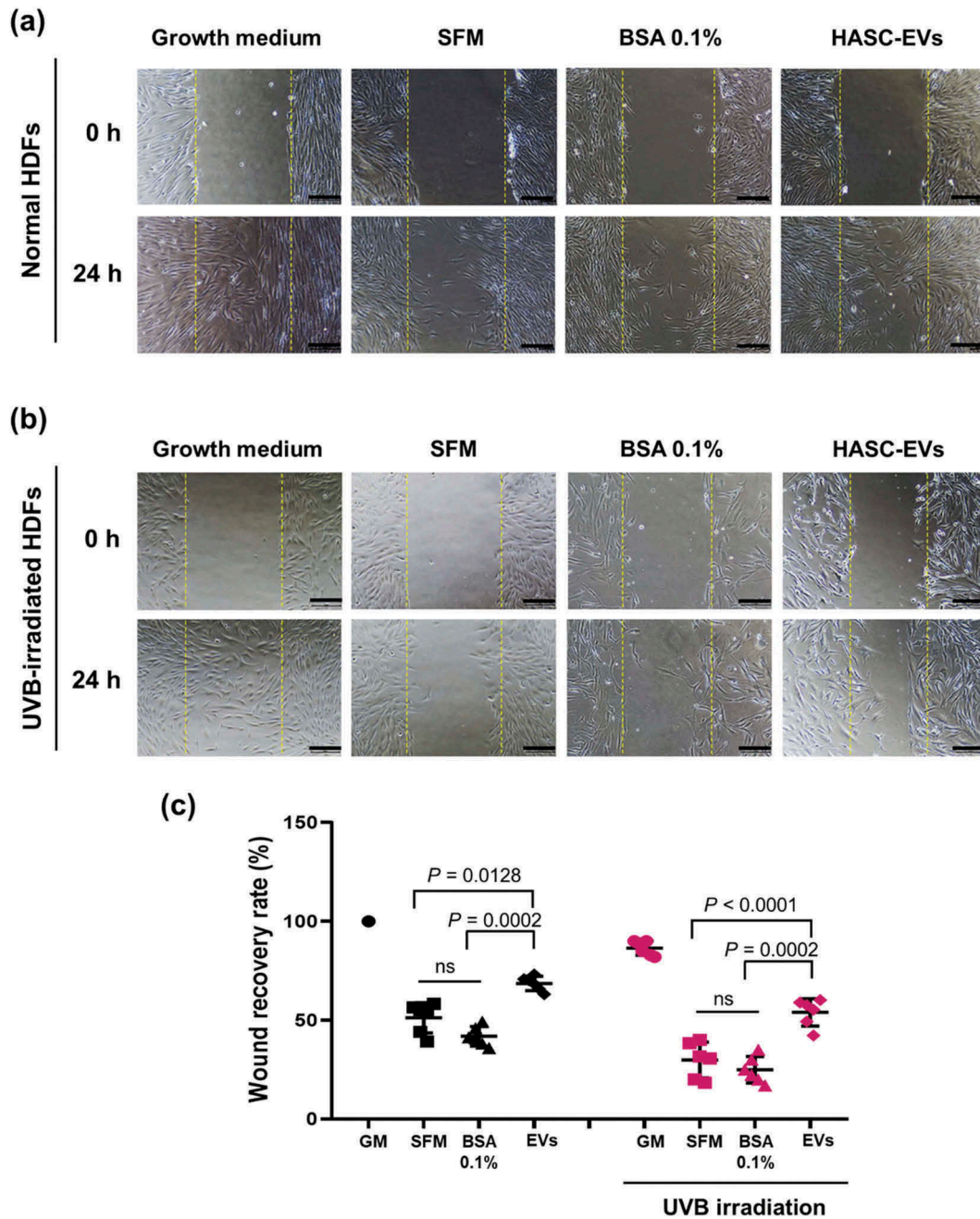
Figure 5. The effects of HASC-derived EVs on the wound recovery of UVB-irradiated HDFs. HDFs were seeded in 24-well plates at 1×10^5 cells per well and maintained in growth medium until they reached 90% confluence. The HDFs were then exposed to UVB radiation at a dose of 0.05 J/cm^2 once a day for 3 days. The normal and UVB-irradiated HDFs were scratch-wounded with a sterilized micropipette tip and incubated in growth medium (GM), serum-free medium (SFM), BSA 0.1% and EVs (1×10^8 particles/mL) containing SFM for 24 h. (a, b) Light microscopic images of HDFs in the scratched area. The yellow dotted lines indicate the original wound edge in the scratch array. Scale bars represent 200 μm. (c) Wound recovery rates of HDFs into the scratched area. The wound recovery rate is presented as the percentage of scratch closure. The data are shown as the means ± standard deviations ($n = 5$).

When HDFs were treated with 50 mJ/cm^2 of UVB radiation, the protein levels of MMP-1 (163.5 ± 30.06%), MMP-3 (120.1 ± 12.7%) and MMP-9 (106.4 ± 3.6%) secreted into the culture media increased compared to non-irradiated HDFs. Treatment with HASC-derived EVs at 1×10^8 particles/mL attenuated the increase in expression of MMP-1 (111.8 ± 5.5%), MMP-3 (101.8 ± 3.4%) and MMP-9 (99.0 ± 2.7%) by UVB irradiation. In addition, the HASC-derived EV treatment significantly increased the levels of type 1 procollagen, type 3 collagen and TIMP-1 decreased by UVB irradiation (type 1 procollagen from 119.6 ± 35.8 to
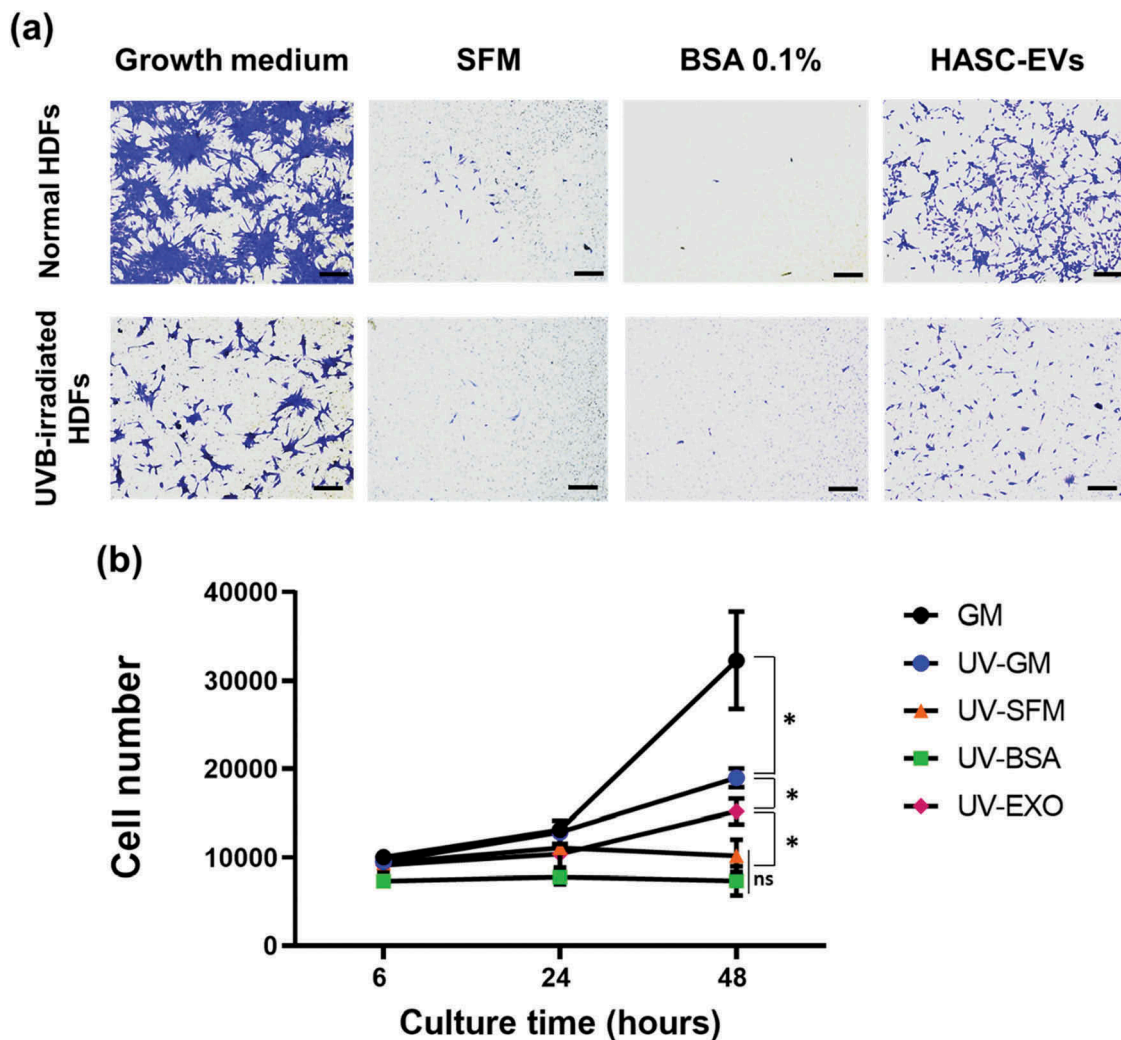
Figure 6. The effects of HASC-derived EVs on the (a) migration and (b) proliferation of UVB-irradiated HDFs. HDFs were exposed to UVB radiation at a dose of 0.05 J/cm^2 once a day for 3 days. (a) The normal and UVB-irradiated HDFs were seeded into the upper side of the transwell membrane and maintained in growth medium (GM), serum-free medium (SFM), BSA 0.1% and EVs (1×10^8 particles/mL) containing SFM for 24 h. Migrated cells to the lower side were fixed with 4% paraformaldehyde and stained with crystal violet. Scale bars represent 100 μm. (b) The normal and UVB-irradiated HDFs were seeded in 24-well plates and maintained in growth medium (GM), serum-free medium (SFM), BSA 0.1% and EVs (1×10^8 particles/mL) containing SFM for 48 h. The proliferation of HDFs was determined by CCK-8 assay. The data are shown as the means ± standard deviations ($n = 4$) with significance at *$p < 0.01$.

262.6 ± 54.1%, type 3 collagen from 61.2 ± 4.5 to 80.8 ± 2.7%, and TIMP-1 from 45.8 ± 7.2 to 73.8 ± 2.9%). Taken together, these results suggest that HASC-derived EVs attenuate UVB-induced MMP expression and promote dermal matrix synthesis by regulating TIMP-1 and TGF-β1 expression.

Discussion

EVs have emerged as a complex means of modulating a variety of cellular processes [29]. Stem cell-derived EVs play a key role in mediating the capacity of stem cells via the delivery of biologically active molecules (eg proteins and RNAs) into recipient cells [30]. Several studies have shown the promise of stem cell-derived EVs in the field of dermatology. For instance, EVs secreted from mesenchymal stem cells (MSCs) help in promoting migration, collagen synthesis in normal or wound fibroblasts, and angiogenesis in human umbilical vein endothelial cells (HUVECs) [18,19,21]. In this study, we demonstrated that HASC-derived EVs promote the functional recovery of dermal fibroblasts damaged by UVB radiation. An in vitro migration and proliferation assay showed that HASC-derived EVs can influence the functional recovery of UVB-damaged HDFs compared with serum-free medium without EVs or with BSA 0.1% (Figures 5 and 6). Although the cell proliferation capacity enhanced by
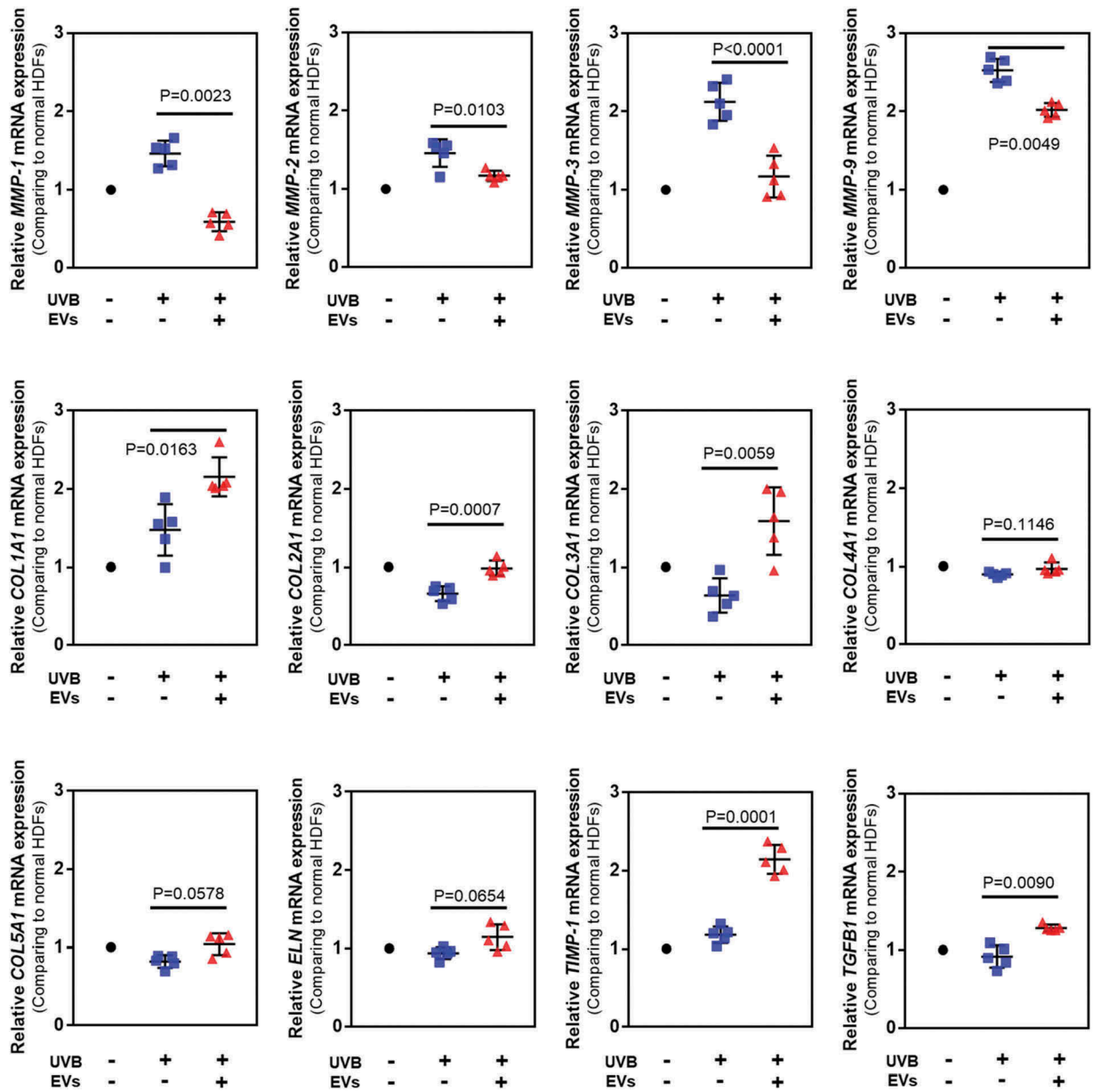
Figure 7. Gene expression in HDFs with or without HASC-derived EVs treatment after UV irradiation. The gene expression was determined using quantitative PCR. Relative gene expression was normalized to a housekeeping gene (*GAPDH*) and expressed as the fold change compared to normal HDFs. The data are shown as the means ± standard deviations (*n* ≥ 5). Abbreviations: *COL1A1*, type I collagen alpha 1; *COL2A1*, type II collagen alpha 1; *COL3A1*, type 3 collagen alpha 1; *COL4*A2, type IV collagen alpha 1; *COL5A1*, type V collagen alpha 1; *ELN*, elastin; *MMP*, matrix metalloproteinase; *TIMP*, tissue inhibitor of metalloproteinase; *TGFB1*, transforming growth factor-β1.

EVs may affect the rate of gap-filling of the scratch wound, the effect of EVs on the migration of HDFs was demonstrated in transwell migration assay. These results indicate that EVs contains key factors to restore the proliferation and migration capacity of damaged HDFs. Quantitative RT-PCR and ELISA analyses revealed that HASC-derived EVs abated the UVB-induced increase in MMPs (MMP-1, -2, -3 and -9) and restored the UVB-induced decrease of collagens (type I, II, III, IV and V), elastin, TIMP-1 and TGF-β1

in dermal fibroblasts (Figures 7 and 8). Indeed, MMPs are particularly important to skin photoaging because of their collagenolytic activity. Among the 18 MMPs expressed in human skin, seven are significantly elevated by UV irradiation, including MMP-1 (collagenase-1, collagen degradation), MMP-2 and MMP-9 (gelatinases A and B, elastin degradation) and MMP-3 (stromelysin 1, collagen and elastin degradation) [31,32]. Therefore, controlling MMP activity is one of the therapeutic strategies for treatment of photoaging.
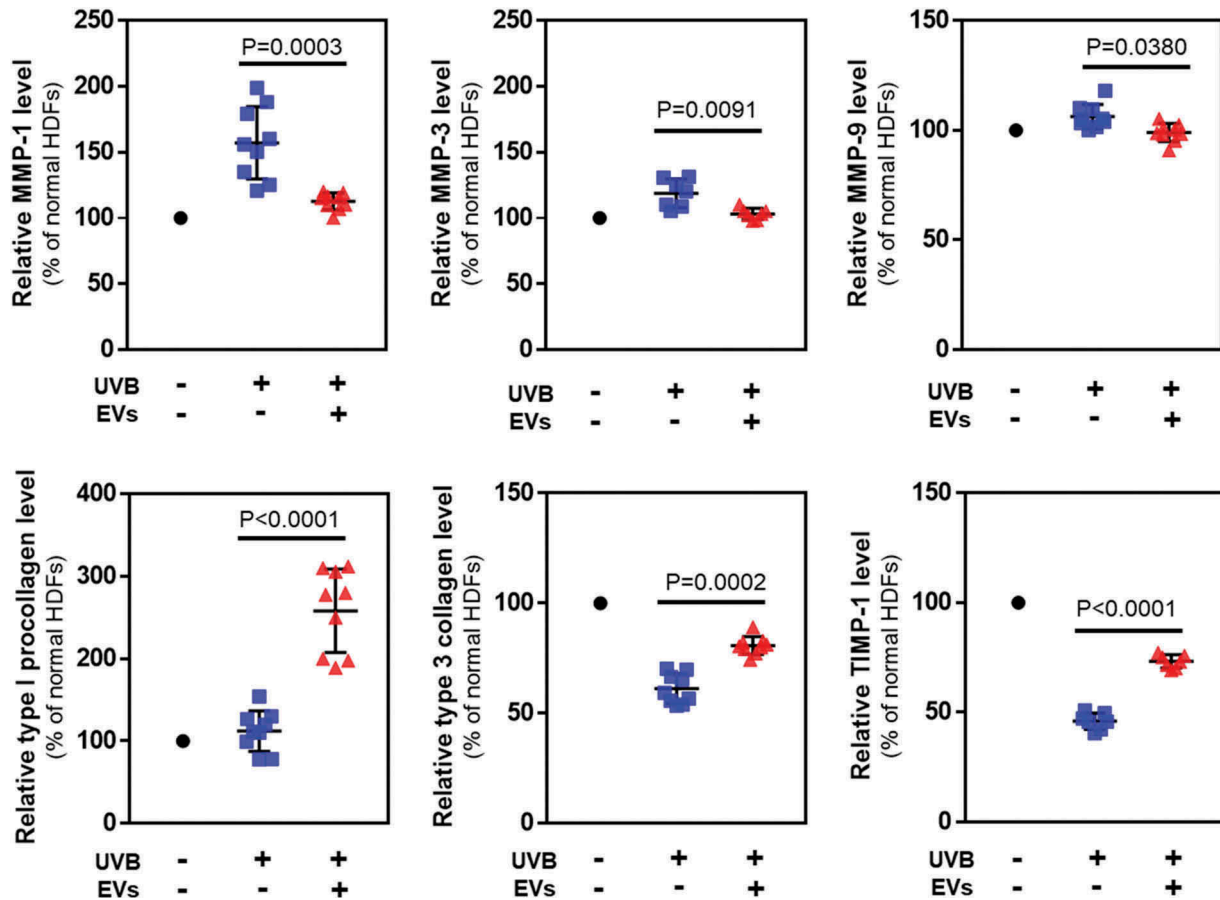
Figure 8. Protein levels in HDFs with or without HASC-derived EVs treatment after UV irradiation. The expression of proteins associated with dermal matrix synthesis and degradation was determined using ELISA. The values were normalized to total protein concentration. The data are shown as the means ± standard deviations ($n \geq 5$).

We hypothesized that miRNAs and proteins have an important influence on the function of dermal fibroblasts damaged by UVB irradiation. We first screened the target genes and corresponding cellular functions of the miRNAs enriched in EVs and performed a functional gene-annotation analysis using the KEGG pathway database (Figure 2). The results showed that the predicted target genes of miRNAs expressed in the EVs are associated with fibroblast proliferation, UV protection, collagen synthesis, DNA repair and cell ageing. Among the expressed miRNAs, several (eg miRNA-135a-5p, miRNA-378h, miRNA-586, miRNA-1972, miRNA-3064-5p, miRNA-3173-5p, miRNA-3613-3p, miRNA-4484, miRNA-4502, miRNA-4507, miRNA-4423-5p, miRNA-4436b-5p, miRNA-4668-3p, miRNA-4726, miRNA-4775, miRNA-4793 and miRNA-6831-5p) are thought to be primarily associated with the TGF-β, MAPK (mitogen-activated protein kinase) and Wnt signalling pathways, which are known to regulate a variety of cellular functions including cell survival, proliferation and collagen synthesis [33,34]. Functional enrichment analysis of the EV proteins also indicated a high representation by ECM proteins and

binding proteins involved in ECM organization as well as proteins involved in enzyme activity, signalling pathway, cell migration and cell proliferation (Figure 3(a)). Interestingly, HASC-derived EVs contained various cytokines, such as IL-1α, -2, -6, -8 and -13, TGF-β1 and –β2, TNF-α and –β, IGF-1, VEGF, PDGF-BB, IGFBP-3 and TIMP-1 and -2 (Figure 3(b)). Of these, IL-1, -2, -6, -8 and -13, as well as EGF, FGF, PDGF-BB and IGFBP, promote the recruitment and proliferation of dermal fibroblasts [35–37]. TNF-α, VEGF, TGF-β and TIMPs are known to regulate ECM protein secretion in dermal fibroblasts [35,38]. Among the detected EV cytokines, it should be noted that TGF-β and TIMPs are potent regulators of ECM synthesis and turnover. TGF-β is one of the key regulators that accelerate the denaturation and/or degradation of collagens and elastic fibres in the dermis by regulating the balance between MMPs and TIMPs [39]. Reactive oxygen species (ROS) generated by UVB irradiation lead to the activation of transcription factors, such as activator protein-1 (AP-1) in dermal fibroblasts. The increased AP-1 activity induces MMP production and inhibits collagen secretion by blocking TGF-β function [3]. Recent studies

have also shown that exogenous TGF-β upregulates many ECM protein genes, such as collagens, elastin, fibronectin and proteoglycans by downregulating MMPs and upregulating TIMPs in UVB-irradiated dermal fibroblasts [27,40,41]. TIMPs are also regulators of dermal matrix turnover. TIMP-1 and -2 mainly inhibit the activity of MMP-1, -2, -3 and -9 [42]. Additionally, numerous studies reported that TIMP-1 and -2 could inhibit apoptosis and promote growth in various cell lines including endothelial cells, hepatic stellate cells, erythroid cells, and fibroblasts [43–46]. These previous findings support our assertion that EV cytokines, in particular TGF-β and TIMP-1 and -2, effectively assist in the recovery of photo-damaged dermal fibroblasts by inhibiting excessive MMP activity and stimulating ECM protein secretion (Supplementary Figure S4). In spite of the obvious effects of HASC-derived EVs, it remains unclear which specific factors in the EVs are primarily responsible for controlling recovery from UVB-induced cell damage due to the complexity of the EV components. Therefore, these issues will be addressed in further studies on identification of candidate EV proteins and their therapeutic efficacy using in vitro and in vivo models. Nonetheless, we highly expect that the various components that are enriched in EVs could synergistically contribute to the functional recovery of UVB-irradiated dermal fibroblasts, and that EVs are a very promising agent for the treatment of photoaging.

We demonstrated that HASC-derived EVs have positive effects on UVB-damaged human dermal fibroblasts in vitro. HASC-derived EVs promoted the migration of UVB-damaged fibroblasts, attenuated the UVB-induced overexpression of MMPs and stimulated dermal matrix production through the transfer of diverse EV components. Therefore, we propose that EVs can contribute to the restoration of UVB-irradiated dermal fibroblasts and are highly promising as an anti-photoaging agent.

Disclosure statement

Funding

References

[1] Ganceviciene R, Liakou AI, Theodoridis A, et al. Skin anti-aging strategies. Dermatoendocrinol. 2012;4 (3):308–319.

[2] Fisher GJ, Kang S, Varani J, et al. Mechanisms of photoaging and chronological skin aging. Arch Dermatol. 2002;138(11):1462–1470.

[3] Cavinato M, Jansen-Dürr P. Molecular mechanisms of UVB-induced senescence of dermal fibroblasts and its relevance for photoaging of the human skin. Exp Gerontol. 2017;94:78–82.

[4] Antoniou C, Kosmadaki MG, Stratigos AJ, et al. Photoaging: prevention and topical treatments. Am J Clin Dermatol. 2010;11(2):95–102.

[5] Permatasari F, Hu YY, Zhang JA, et al. Anti-photoaging potential of Botulinum Toxin Type A in UVB-induced premature senescence of human dermal fibroblasts in vitro through decreasing senescence-related proteins. J Photochem Photobiol B. 2014;133:115–123.

[6] Huh WB, Kim JE, Kang YG, et al. Brown pine leaf extract and its active component trans-communic acid inhibit UVB-induced MMP-1 expression by targeting PI3K. PLoS One. 2015;10(6):e0128365.

[7] Kim WS, Park BS, Kim HK, et al. Evidence supporting antioxidant action of adipose-derived stem cells: protection of human dermal fibroblasts from oxidative stress. J Dermatol Sci. 2008;49(2):133–142.

[8] Kim WS, Park BS, Park JS, et al. Antiwrinkle effect of adipose-derived stem cell: activation of dermal fibroblast by secretory factors. J Dermatol Sci. 2009;53(2):96–102.

[9] Masaki H. Role of antioxidants in the skin: anti-aging effects. J Dermatol Sci. 2010;58(2):85–90.

[10] Lohani A, Verma A, Joshi H, et al. Nanotechnology-based cosmeceuticals. ISRN Dermatol. 2014;2014:843687.

[11] Lee CM. Fifty years of research and development of cosmeceuticals: a contemporary review. J Cosmet Dermatol. 2016;15(4):527–539.

[12] Andaloussi S EL, Mager I, Xo B, et al. Extracellular vesicles: biology and emerging therapeutic opportunities. Nat Rev Drug Discov. 2013;12(5):347–357.

[13] Yáñez-Mó M, Siljander PR, Andreu Z, et al. Biological properties of extracellular vesicles and their physiological functions. J Extracell Vesicles. 2015;4:27066.

[14] Schorey JS, Bhatnagar S. Exosome function: from tumor immunology to pathogen biology. Traffic. 2008;9 (6):871–881.

[15] Thery C, Zitvogel L, Amigorena S. Exosomes: composition, biogenesis and function. Nat Rev Immunol. 2002;2 (8):569–579.

[16] Vishnubhatla I, Corteling R, Stevanato L, et al. The development of stem cell-derived exosomes as a cell-free regenerative medicine. J Circ Biomark. 2014;3(2):1–14.

[17] Yang Y, Hong Y, Cho E, et al. Extracellular vesicles as a platform for membrane-associated therapeutic protein delivery. J Extracell Vesicles. 2018;7(1):1440131.

[18] Zhang J, Guan J, Niu X, et al. Exosomes released from human induced pluripotent stem cells-derived MSCs facilitate cutaneous wound healing by promoting collagen synthesis and angiogenesis. J Transl Med. 2015;13(49):1–14.

[19] Shabbir A, Cox A, Rodriguez-Menocal L, et al. Mesenchymal stem cell exosomes induce proliferation and migration of normal and chronic wound fibroblasts, and enhance angiogenesis in vitro. Stem Cells Dev. 2015;24(14):1635–1647.

[20] Zhang J, Chen C, Hu B, et al. Exosomes derived from human endothelial progenitor cells accelerate cutaneous wound healing by promoting angiogenesis through Erk1/2 signaling. Int J Biol Sci. 2016;12(12):1472–1487.

[21] Hu L, Wang J, Zhou X, et al. Exosomes derived from human adipose mensenchymal stem cells accelerates cutaneous wound healing via optimizing the characteristics of fibroblasts. Sci Rep. 2016;6:32993.

[22] Fang S, Xu C, Zhang Y, et al. Umbilical cord-derived mesenchymal stem cell-derived exosomal microRNAs suppress myofibroblast differentiation by inhibiting the transforming growth factor-β/SMAD2 pathway during wound healing. Stem Cells Transl Med. 2016;5(10):1425–1439.

[23] Huang P, Bi J, Owen GR, et al. Keratinocyte microvesicles regulate the expression of multiple genes in dermal fibroblasts. J Invest Dermatol. 2015;135(12):3051–3059.

[24] Li P, Kaslan M, Lee SH, et al. Progress in exosome isolation technique. Theranostic. 2017;7(3):789–804.

[25] Heinemann ML, Ilmer M, Silva LP, et al. Benchtop isolation and characterization of functional exosomes bysequential filtration. J Chromatogr A. 2014;1371:125–135.

[26] Lai RC, Arslan F, Lee MM, et al. Exosome secreted by MSC reduces myocardial ischemia/reperfusion injury. Stem Cell Res. 2010;4(3):214–222.

[27] Yokose U, Hachiya A, Sriwiriyanont P, et al. The endogenous protease inhibitor TIMP-1 mediates protection and recovery from cutaneous photodamage. J Invest Dermatol. 2012;132(12):2800–2809.

[28] Pan X, Chen Z, Huang R, et al. Transforming growth factor β1 induces the expression of collagen type I by DNA methylation in cardiac fibroblasts. PLoS One. 2013;8(4):e60335.

[29] McBride JD, Rodriguez-Menocal L, Badiavas EV. Extracellular vesicles as biomarkers and therapeutics in dermatology: a focus on exosomes. J Invest Dermatol. 2017;137(8):1622–1629.

[30] Motavaf M, Pakravan K, Babashah S, et al. Therapeutic application of mesenchymal stem cell-derived exosomes: A promising cell-free therapeutic strategy in regenerative medicine. Cell Mol Biol. 2016;62(7):74–79.

[31] Quan T, Little E, Quan H, et al. Elevated matrix metalloproteinases and collagen fragmentation in photodamaged human skin: impact of altered extracellular matrix microenvironment on dermal fibroblast function. J Invest Dermatol. 2013;133(5):1362–1366.

[32] Pittayapruek P, Meephansan J, Prapapan O, et al. Role of matrix metalloproteinases in photoaging and photocarcinogenesis. Int J Mol Sci. 2016;17(6):868–888.

[33] Akhmetshina A, Palumbo K, Dees C, et al. Activation of canonical Wnt signalling is required for TGF-β-mediated fibrosis. Nat Commun. 2012;3:735.

[34] He W, Dai C. Key fibrogenic signaling. Curr Pathobiol Rep. 2015;3(2):183–192.

[35] Kendall RT, Feghali-Bostwick CA. Fibroblasts in fibrosis: novel roles and mediators. Front Pharmacol. 2014;5(123):1–13.

[36] Li W, Fan J, Chen M, et al. Mechanism of human dermal fibroblast migration driven by type I collagen and platelet-derived growth factor-BB. Mol Biol Cell. 2004;15(1):294–309.

[37] Edmondson SR, Thumiger SP, Werther GA, et al. Epidermal homeostasis: the role of the growth hormone and insulin-like growth factor systems. Endocr Rev. 2003;24(6):737–764.

[38] Shah JM, Omar E, Pai DR, et al. Cellular events and biomarkers of wound healing. Indian J Plast Surg. 2012;45(2):220–228.

[39] Lin PS, Chang HH, Yeh CY, et al. Transforming growth factor beta 1 increases collagen content, and stimulates procollagen I and tissue inhibitor of metalloproteinase-1 production of dental pulp cells: role of MEK/ERK and activin receptor-like kinase-5/Smad signaling. J Formos Med Assoc. 2017;116(5):351–358.

[40] Verrecchia F, Chu ML, Mauviel A. Identification of novel TGF-beta/Smad gene targets in dermal fibroblasts using a combined cDNA microarray/promoter transactivation approach. J Biol Chem. 2001;276(20):17058–17062.

[41] Verrecchia F, Mauviel A. Transforming growth factor-beta signaling through the Smad pathway: role in extracellular matrix gene expression and regulation. J Invest Dermatol. 2002;118(2):211–215.

[42] Baker AH, Edwards DR, Murphy G. Metalloproteinase inhibitors: biological actions and therapeutic opportunities. J Cell Sci. 2002;115(Pt19):3719–3727.

[43] Boulday G, Fitau J, Coupel S, et al. Exogenous tissue inhibitor of metalloproteinase-1 promotes endothelial cell survival through activation of the phosphatidylinositol 3-kinase/Akt pathway. Ann N Y Acad Sci. 2004;1030:28–36.

[44] Murphy FR, Issa R, Zhou X, et al. Inhibition of apoptosis of activated hepatic stellate cells by tissue inhibitor of metalloproteinase-1 is mediated via effects on matrix metalloproteinase inhibition: implications for reversibility of liver fibrosis. J Biol Chem. 2002;277(13):11069–11076.

[45] Lambert E, Boudot C, Kadri Z, et al. Tissue inhibitor of metalloproteinases-1 signalling pathway leading to erythroid cell survival. Biochem J. 2003;372(Pt3):767–774.

[46] Guo XK, Zhao WQ, Kondo C, et al. Tissue inhibitors of metalloproteinases-1 (TIMP-1) and −2 (TIMP-2) are major serum factors that stimulate the TIMP-1 gene in human gingival fibroblasts. Biochim Biophys Acta. 2006;1763(3):296–304.